Ultrathick MoS_2 Films with Exceptionally High Volumetric Capacitance

Zheng Bo (bozh@zju.edu.cn)
Zhejiang University https://orcid.org/0000-0001-9308-7624

Xiangnan Cheng
Zhejiang University

Huachao Yang
Zhejiang University

Xinzheng Guo
Zhejiang University

Jianhua Yan
State Key Laboratory of Clean Energy Utilization, Department of Energy engineering, Zhejiang University

Kefa Cen
Zhejiang University

Zhaojun Han
Commonwealth Scientific and Industrial Research Organisation

Liming Dai
University of New South Wales

Article

Keywords: miniaturized supercapacitor systems, electrode films, submillimeter thickness, volumetric performance, solvated-ion-intercalated hydrothermal strategy

Posted Date: August 17th, 2021

DOI: https://doi.org/10.21203/rs.3.rs-777887/v1

Abstract

Manufacturing electrode films at an industrial-level submillimeter thickness (~ 100 μm) with superior volumetric performance is of practical significance for the commercialization of miniaturized supercapacitor systems. Herein, we propose a commercially scalable solvated-ion-intercalated hydrothermal strategy to demonstrate a recorded-high volumetric capacitance (511.29 F cm^{-3}) for supercapacitors based on industrial-level submillimeter MoS_2 film electrode (94.2 μm). The intercalated solvated-Li^+ ions increase the amount of negative surface charges and reduce the formation energy of 1T MoS_2, leading to a high metallic phase purity of 82.7% with enhanced electrical conductivity. Together with the expanded interlayer distance (~ 1.23 nm), this allows rapid electron transfer and ion transport in the excessively-stacked ultrathick MoS_2 film to be simultaneously realized. Thus, the as-fabricated MoS_2||activated carbon asymmetric supercapacitor presents both high energy and power densities, outperformed those of commercial devices, including supercapacitors with submillimeter-thick electrodes and even micrometer-thick electrodes.

Introduction

Owing to their high power density and excellent cyclability, supercapacitors are attractive energy storage devices for portable electronics, smart power grids, electric vehicles, and even renewable energy sources for large-scale deployment[1-7]. Due to their widely-recognized large surface area, high packing density and excellent electrical conductivity, two-dimensional (2D) nanomaterials are of particular interest as new electrodes for supercapacitors with high volumetric performance, which is a more pertinent figure-of-merit than the traditionally used gravimetric performance, particularly for miniaturized and portable supercapacitor devices[8-12]. So far, high volumetric capacitances have been achieved in the micrometer-thick electrodes of 2D nanomaterials, e.g., ~1500 F cm^{-3} for a 3-μm-thick transition metal carbides (MXene) film[12], 1445 F cm^{-3} for a ~3.3-μm-thick MXene/graphene film[13], ~700 F cm^{-3} for a 5-μm-thick MoS_2 film[14], and ~572 F cm^{-3} for a 7.8-μm-thick graphene/polyaniline (PANI) composite[15], which significantly overwhelm the traditional activated carbon counterpart (60~100 F cm^{-3} at a similar thickness[16]). However, aiming at industrial real applications, a submillimeter electrode thickness of ~100 μm is essentially required[2,4,17]. For 2D nanomaterials, an increase of film thickness from micrometer to submillimeter level usually causes severely deteriorated performance[18]. As such, development of 2D nanomaterial electrodes with high volumetric performance at an industrial-level thickness is of particular importance and has recently attracted great attention[16,19,20].

The tremendous interest in using MoS_2 as the miniaturized supercapacitor electrodes stems from its high electrochemical activity derived from its variable Mo oxidation states and abundant active edge S atoms, well-aligned layered structure, and high accessible surface area[8,21,22]. Although Acerce *et al.*[14] have successfully demonstrated a superior volumetric capacitance of ~700 F cm^{-3} for micrometer thick MoS_2, the thickness (5 μm) cannot meet the requirements of industrial applications. To the best of our

knowledge, MoS_2 film at submillimeter thickness with a high volumetric capacitance has not yet been reported, and its commercial application for energy storage is still precluded. Two critical issues need to be addressed in order to achieve the high volumetric capacitance for MoS_2, especially at an industrial-level submillimeter thickness: i) the low conductivity which is strongly limited by its low metallic 1T phase purity. Generally, MoS_2 has a 2H phase crystal structure with semi-insulating property and a 1T phase crystal structure with superior electrical conductivity (10^7 times more conductive than that of the semiconducting 2H phase)[8,14,21,23]. MoS_2 nanosheets prepared by the conventional organic lithium intercalation[14,24-27] and hydrothermal strategies[28-30] usually have a 1T phase purity less than 70%, leading to poor electron transfer rate, high electrical resistance, and relatively low volumetric capacitance, especially for thick films. Moreover, the metastable 1T phase is easily converted to the stable 2H phase[31], which significantly restricts the practical applications; ii) the sluggish ion kinetics and few accessible active sites which are intrinsically associated with conventional 2D nanomaterials. Due to the interlayer agglomeration (or the excessive nanosheets stacking in MoS_2), thick MoS_2 films inevitably result in a lengthy ion diffusion path and high transport resistance, declining the utilization of built-in active sites and charge storage capability.

Herein, we report a solvated-ion-intercalated hydrothermal strategy to simultaneously address the above challenges, achieving a recorded-high volumetric capacitance (511.29 F cm^{-3}) for supercapacitors based on submillimeter MoS_2 film electrode (94.2 μm). In our approach, the solvated lithium intercalation increases the negative charges on the MoS_2 nanosheets, leading to a lowered formation energy for 1T phase. The metallic 1T phase purity of the as-fabricated MoS_2 nanosheets thus reaches 82.7% (remains at 72.73% after 60 days), which is significantly higher than that of their counterparts from traditional hydrothermal methods[28-30,32], and is comparable to those from the chemical vapor deposition (CVD) routes[33]. In addition to the high 1T phase purity, the as-fabricated MoS_2 nanosheets also show an expanded interlayer spacing (from ~0.62 to ~1.23 nm), a rapid electron transfer, an unimpeded ion transport, and a reduced ion diffusion distance. As a result, the 1.45-μm-thick and 9.30-μm-thick MoS_2 films reach volumetric capacitances as high as 1054.5 and 809.3 F cm^{-3}, respectively. A high volumetric capacitance of 511.29 F cm^{-3} can still be achieved for the 94.2-μm-thick MoS_2 film, which is among the best values reported in the literature for submillimeter thick electrodes[12,16,19,20]. The as-fabricated MoS_2||activated carbon asymmetric supercapacitor exhibits both high volumetric energy and power densities of ~14.4 mWh cm^{-3} and ~12.86 W cm^{-3}, respectively, outperformed those of commercial devices, including supercapacitors with submillimeter-thick electrodes and even micrometer-thick electrodes.

Fabrication Of High-purity 1t-phase Mos2

In this work, we developed a solvated-ion-intercalated hydrothermal method to fabricate MoS_2 nanosheets. Briefly, solvated lithium ions are introduced as the intercalator during the hydrothermal reaction of ammonium molybdate (Mo source) and thioacetamide (S source) in a Teflon-lined stainless

autoclave (see Methods). Apart from the inherent advantages of hydrothermal strategies[28,29] (e.g., easily scale-up, time-effective and mild reactions without hazardous organics), the newly-developed method can realize a much higher 1T purity of MoS_2 (up to 82.7%) with a significantly improved phase stability (purity of 72.3% after 60 days) over traditional hydrothermal methods.

A key feature of the newly-developed method is that solvated alkali metal ions (e.g., lithium ions) are intercalated into the interlayer spacing of MoS_2 nanosheets during the hydrothermal reactions. In the traditional hydrothermal processes, 1T MoS_2 nanosheets are generally prepared by Mo source (e.g., ammonium molybdate and molybdenum trioxide) and S source (e.g., thioacetamide and thiourea) through the reduction reactions induced by the reducibility of the S precursors, as shown in Fig. 1a. However, it suffers from the poor reduction rate and limited metallic phase purity. Inspired by the reduced formation energy of 1T-phase MoS_2 through introducing alkali metal ions in the CVD processes[34], we added Li_2SO_4 solution into the hydrothermal reactions in this work (Fig. 1a). The solvated lithium intercalation can increase the negative charges on MoS_2 nanosheets, leading to lowered formation energy of metallic phase for a high 1T purity (Fig. 1b). Meanwhile, the interlayer spacing is expanded after the solvated-ion-intercalation. The as-proposed new method is scalable through a rolling process (Methods) and align well with commercialization, which is demonstrated by a ~70 cm × 7 cm 1T MoS_2 film with a submillimeter thickness (Fig. 1c).

Materials Characterization And Formation Mechanism

Quantitative information of 1T phase purity is estimated based on the deconvolution of X-ray photoelectron spectroscopy (XPS) peaks. As shown in Fig. 2a, the Mo 3*d* of 1T phase exhibits two strong peaks at 228.0 (Mo $3d_{5/2}$) and 231.2 eV (Mo $3d_{3/2}$), which are shifted to the lower binding energy (by ~1.2 eV) in comparison with the 2H phase (229.2 eV and 232.4 eV respectively). The corresponding peak deconvolution of Mo 3*d* reveals the content of 1T and 2H phase[30,31,34,35]. It is observed that with the increase of Li^+ concentration, the 2H phase (blue regions in Fig. 2a) of the Li^+-intercalated MoS_2 nanosheets decreases accordingly. In comparison with the traditional hydrothermal strategy, the solvated lithium intercalation remarkably improves the 1T phase purity from 65.1% to up to 82.7%, which increases with the increasing Li^+ concentration of the precursor solution from 0.5 M to 1.5 M. The high metallic phase purity is also confirmed by the Raman peaks at 151.28, 216.74, 324.76 and 408.47 cm^{-1} for 1T MoS_2 nanosheets (Supplementary Fig. 1), agreeing well with previously reported Raman results[30,31,33,35].

The improved 1T phase purity can be attributed to the lowered formation energy of the 1T phase, which is induced by the increased negative charges on the MoS_2 nanosheets after the solvated lithium intercalation. Transmission electron microscope (TEM) images are used to reveal the successful intercalation of solvated lithium ions. As shown in Fig. 2b, the interlayer spacings of the Li^+-intercalated MoS_2 nanosheets are 1.04, 1.15 and 1.23 nm, corresponding to the Li^+ concentrations of 0.5, 1 and 1.5 M,

respectively, which are higher than those of MoS_2 nanosheets prepared from the traditional hydrothermal method (0.88 nm) and the typical value of closely packed MoS_2 (~0.62 nm)[25]. It proves the intercalation of solvated lithium ions. Zeta potential measurements are performed to investigate the change of negative charges on the MoS_2 nanosheets after the intercalation of solvated lithium ions. The average zeta potential of MoS_2 nanosheets from the solvated-ion-intercalation method (1.5 M Li^+ ions) is -38.1 mV, which is higher than that of MoS_2 nanosheets (-32.0 mV) from the traditional hydrothermal strategy (Fig. 2c). These results reveal that the solvated lithium intercalation is able to increase the amount of negative charges on the MoS_2 nanosheets.

Density functional theory (DFT) calculations are performed to reveal the influence of negative charges on the formation energy of 1T phase. Spin-polarized DFT calculations are conducted with generalized gradient approximation[36] based on the Perdew-Burke-Ernzerhof[37] functions. The energy and force convergence criteria are set to 1×10^{-5} eV and 1×10^{-2} eV/Å, respectively, with an energy cutoff of 400 eV (see Methods). Fig. 2d shows the 4 × 4 super cells of 1T and 2H phase MoS_2 structures for the DFT calculations. The optimized geometric structures are consistent with the previous simulation studies[38]. As shown in Fig. 2e, the difference in formation energy between 1T and 2H phases of MoS_2 decreases from 13.48 to -4.47 eV with increasing surface charge density, indicating that the formation of 1T phase MoS_2 becomes easier than that of 2H phase after the solvated lithium intercalation, which is probably attributed to the electron filling of the *d* orbits of Mo atoms[31].

Since the metastable 1T phase is easily converted into the 2H phase[31,39], the phase stability of 1T MoS_2 nanosheets is another critical issue for real applications. As shown in Fig. 2f, the 1T purity of the Li^+-intercalated MoS_2 nanosheets decreases from 82.7% to 72.73% with a high retention ratio of 87.9%, and the corresponding aqueous dispersion remains stable without obvious precipitation after 60 days. In contrast, the phase purity of samples made from the traditional hydrothermal method decays significantly (1T purity from 65.1% to 47.97% after 60 days with a retention ratio of 73.6%). Meanwhile, particle precipitation can be easily seen after the first 24 hours (Supplementary Fig. 2), due to the severe restacking of 2H MoS_2 nanosheets with a poor wettability[28].

Submillimeter-thick Mos2 Film With High Volumetric Capacitance

The high metallic 1T phase purity and expanded interlayer spacing could facilitate fast electron transfer and rapid ion transport, as demonstrated by the excellent volumetric capacitive performance for micrometer- and submillimeter-thick MoS_2 films. As shown in Figs. 3a, d and g, 1.45 μm-, 9.30 μm- and 94.2 μm-thick MoS_2 films are fabricated through the newly-developed solvated-ion-intercalated hydrothermal method. Electrochemical measurements are firstly conducted on the as-fabricated filtrated MoS_2 film with a thickness of 1.45 μm in 1.0 M Li_2SO_4 aqueous electrolyte (Fig. 3a and Supplementary Fig. 3). Control experiments are conducted on the MoS_2 film generated by the traditional hydrothermal method (Supplementary Fig. 4). Based on the cyclic voltammetry (CV) measurements at a scan rate of 20

mV s^{-1} (Fig. 3b, solid lines), the capacitance C consists of two contributions[40] ($C = k_1 + k_2 v^{-0.5}$), i.e., rate-independent component k_1 (surface capacitive effects, Fig. 3b, dashed lines) and diffusion-limited capacitance k_2 dependent on the scan rate v. The Li^+-intercalated MoS_2 film shows substantially-high surface capacitive contributions (~85.2%), superior to its counterpart from the traditional hydrothermal method (~57.5%). These results indicate a better accessibility to the active sites of MoS_2 nanosheets with an expanded interlayer spacing and high 1T phase purity. Moreover, CV profiles can be obtained at a high scan rate of 1000 mV s^{-1}, and the ideal capacitive behavior is further confirmed by GCD curves at the current densities up to 100 A g^{-1} (Supplementary Fig. 3). The electrochemical impedance spectroscopy (EIS) for the Li^+-intercalated MoS_2 film (inset of Fig. 3c) confirmed the reduced equivalent series resistance (R_s) and negligible charge transfer resistance (R_{ct}). The equivalent circuit fitting results (Supplementary Fig. 5) show that the R_{ct} and R_s are 0.45 and 0.78 Ω cm^2, respectively, which are significantly lower than those of the MoS_2 film from the traditional hydrothermal method (3.45 and 2.94 Ω cm^2, respectively). As a result, the Li^+-intercalated MoS_2 film presents a much higher volumetric capacitance of 1054.5 F cm^{-3} (at a scan rate of 5 mV s^{-1}) with improved rate performance (Fig. 3c). The Li^+-intercalated MoS_2 film also shows a high volumetric capacitance of 536.2 F cm^{-3} at a high scan rate of 1000 mV s^{-1}, which is substantially higher than that of the counterpart from the traditional hydrothermal method (72.59 F cm^{-3} at 1000 mV s^{-1}).

In general, the increase in film thickness causes sluggish ion diffusion and reduces charge storage capability, resulting in a significant decrease in the volumetric capacitance[2,18]. In our work, however, the excellent volumetric capacitive performance is mostly retained for thicker Li^+-intercalated MoS_2 film (9.30 μm). As shown in Figs. 3d-f, the 9.30-μm-thick MoS_2 film exhibits a slightly declined volumetric capacitance (809.3 F cm^{-3}) as compared to the 1.45-μm-thick film. Moreover, the volumetric capacitance of our 9.30-μm-thick film is largely superior to the previously reported 5-μm-thick 1T MoS_2 film prepared by the organolithium chemistry method[14].

Moreover, the 94.2-μm-thick 1T MoS_2 film (Fig. 3g), which is prepared by a rolling process through mixing the Li^+-intercalated MoS_2 powder with polytetrafluoroethylene at a ratio of 9 : 1 (see Methods), still exhibits excellent volumetric and areal capacitances of up to 511.29 F cm^{-3} and 4.82 F cm^{-2}, respectively (Fig. 3h). The CV curves from 5 to 100 mV s^{-1} and EIS measurement can be found in Supplementary Fig. 6. As shown in Fig. 3i, these values are higher than those of different 2D nanomaterials at a submillimeter thickness (e.g., 490 F cm^{-3} and 4.21 F cm^{-2} for 86-μm-thick N-doped mesoporous carbon[20], 450 F cm^{-3} and 5.40 F cm^{-2} for 120-μm-thick graphene/PANI composite[19], 88 F cm^{-3} and 1.58 F cm^{-2} for 180-μm-thick microporous MXene film[12] and 330 F cm^{-3} and 2.48 F cm^{-2} for 75-μm-thick MXene film[16]).

Submillimeter-thick Mos2 Film Supercapacitor

To demonstrate the potential practical applications, an asymmetric MoS_2||activated carbon supercapacitor is fabricated with submillimeter-thick MoS_2 film and activated carbon film as the cathode and the anode, respectively, 1.0 M Li_2SO_4 as the electrolyte, and a glass fiber as the separator (Fig. 4a). The galvanostatic charge/discharge (GCD) curves from 0.1 to 5 A g^{-1} and the CV curves are presented in Fig 4b and Supplementary Fig. 7a, respectively. As shown in Fig. 4b, the asymmetric supercapacitor exhibits a volumetric capacitance of 46.1 F cm^{-3} at 0.1 A g^{-1}. According to the EIS tests (Supplementary Fig. 7b), the asymmetric supercapacitor shows typical capacitive characteristics. Ragone plot in Fig. 4c shows a comparison of the volumetric energy and power densities between our device and previous studies. At a current density of 0.1 A g^{-1}, the volumetric energy density is calculated to be ~14.4 mWh cm^{-3} with the corresponding volumetric power density of ~0.13 W cm^{-3}. At a higher current density of 10 A g^{-1}, our device shows a volumetric energy density of ~5.4 mWh cm^{-3} and a volumetric power density of ~12.86 W cm^{-3}. These results outperform the commercially available devices (e.g., 4 V/500 μAh Li thin film battery[41]; 3 V/300 μF electrolytic capacitor[11]; 2.75 V/44 mF and 5.5 V/100 mF commercial supercapacitors[11,42]), as well as supercapacitors with submillimeter-thick electrodes (e.g., ~150 μm activated carbon fibers[17], ~39 μm reduced graphene oxide/carbon nanotube electrode[43], ~20 μm MXene paper electrode[44], and ~18 μm porous carbon electrode[45]) and some micrometer-thick electrodes (e.g., 2.5-μm-thick MXene/graphene[46], 0.58-μm-thick reduced graphene[47] and 3-μm-thick MoS_2/reduced graphene[28]). Moreover, our device exhibits high capacitance retention of 91.6% after 12,000 charge/discharge cycles at a current density of 5 A g^{-1}, demonstrating excellent cyclic stability (Fig. 4d). The outstanding performances can be attributed to the rapid electron transfer and unimpeded ion transport induced by the expanded interlayer spacing and high 1T phase purity after solvated lithium intercalation.

Conclusions

We have demonstrated a solvated-ion-intercalated hydrothermal strategy to prepare MoS_2 nanosheets with a high metallic 1T phase purity, which are promising for the preparation of industrial-level submillimeter MoS_2 films with high volumetric capacitance. The solvated Li^+ ion not only expanded the interlayer spacing of MoS_2 nanosheets, but also increased the negative charges on the MoS_2 nanosheets and reduced the formation energy of 1T phase, leading to the fast electron transfer and ion transport for submillimeter MoS_2 films. Benefited from these advantages, high volumetric and areal capacitances of 511.29 F cm^{-3} and 4.82 F cm^{-2} can still be achieved, which is among the best records reported for submillimeter-thick electrodes. The as-fabricated MoS_2||activated carbon asymmetric supercapacitor exhibits high volumetric energy and power densities of ~14.4 mWh cm^{-3} and ~12.86 W cm^{-3}, respectively, as well as good cycling stability with capacitance retention of 91.6% even after 12,000 cycles, demonstrating the great potential of submillimeter 1T MoS_2 film for commercial supercapacitors.

Methods

Preparation of 1T MoS_2 by the solvated-ion-intercalated strategy and the traditional hydrothermal strategy. Ammonium molybdate ($(NH_4)_6Mo_7O_{24}{\cdot}4H_2O$) and thioacetamide ($CH_3CSNH_2$) were obtained from Shanghai Macklin Biochemical LTD. Lithium sulfate (Li_2SO_4) was purchased from Shanghai Aladdin Biochemical Technology LTD. Urea (CH_4N_2O) was purchased from Sinopharm Chemical Reagent LTD. All other reagents, including deionized water, were purchased commercially and utilized without any special pre-treatment.

To prepare the pristine 1T MoS_2 samples by the traditional hydrothermal strategy, 25 mg ammonium molybdate, 30 mg thioacetamide and 100 mg urea were mixed in 25 mL deionized water followed by 2 h magnetic stirring at 600 rpm. Then, the mixed solution was transferred into a Teflon-lined stainless autoclave and kept in a furnace at 180 °C for 18 h. Subsequently, the autoclave was cooled down to room temperature rapidly by continuous water flow, and then further stabilized at 4 °C for 2 h. The as-prepared samples were collected after centrifugation and washing with deionized water and ethanol for several times, which remove the relatively large nanoparticles and retained the few-layer nanosheets in the dispersion. After 30 min ultrasonic treatment, the 1T MoS_2 samples were stably dispersed in deionized water and kept at 4 °C environment for long-term storage. To prepare Li^+-intercalated 1T MoS_2 samples, 0.275 g, 0.550 g and 0.825 g of lithium sulfate were added into the well-mixed precursor solution mentioned above, which was continuously to stirred at 600 rpm for another 0.5 h. Therefore, the concentration of Li^+ ion in the mixed precursor is 0.5 M, 1.0 M and 1.5 M.

Material characterization. The microstructures of samples were characterized by scanning electron microscope (SEM) (Hitachi SU-70) and transmission electron microscope (TEM) (JEOL JEM-2100). Raman spectra were measured by Raman spectrometer (LabRAM HR Evolution) with a 532 nm excitation wavelength. X-ray photoelectron spectroscopy (XPS) (Escalab Mark II, VG) with a monochromatic Mg Ka X-ray source (1253.6 eV) was used to obtain XPS data. Before Raman and XPS characterization, the 1T MoS_2 dispersion was drop casted on a quartz plate and dried naturally at room temperature.

Density functional theory calculations. The relative stability of 1T and 2H MoS_2 is obtained from density functional theory simulations, performed using Vienna ab initio simulation package (VASP)[48,49] with generalized gradient approximation[36] based on Perdew-Burke-Ernzerhof[37] functions. The energy and force convergence criteria are set to 1×10^{-5} eV and 1×10^{-2} eV/Å, respectively, with an energy cutoff of 400 eV. A k-point mesh of 5 × 5 × 1 is applied to the Brillouin zone within Monkhorst–Pack grids. The relative stability of 1T MoS_2 compared to 2H MoS_2 ($E_s(c)$) is calculated using:

$$E_s(c) = E_t(c) - E_H(c), \quad (1)$$

where $E_T(c)$ and $E_H(c)$ represent the total energy of 1T and 2H MoS_2 with lithium adsorbed, and c is the surface charge density.

Preparation of MoS_2 electrodes and asymmetric supercapacitor. To prepare thin-film electrodes, 1T MoS_2 dispersion was filtered over membranes (25 nm-diameter pore size) and peeled off after drying in vacuum at 50 °C. The film thickness varied from ~1.45 to 9.30 μm depending on the amount of filtered dispersion, with the mass loading ranging from ~0.96 to 5.58 mg cm^{-2}. To prepare submillimeter-thick film electrodes, the MoS_2 dispersion was freeze-dried to obtain 1T MoS_2 powder. It is worth noting that when the freeze-dried ice just completes the sublimation, the remaining powder is collected immediately to avoid the loss of water molecules between the MoS_2 nanosheets. After manually stirring the mixture of 1T MoS_2 powder and polytetrafluoroethylene (PTFE) with a ratio of 9 : 1 for over 3 hours, the well-mixed slurry was rolled, freeze-dried and pressed into film electrodes with the high mass loading of 36.7 mg cm^{-2} and thickness of 94.2 μm. The high packing density is mainly due to the high molecular weight of MoS_2 and the compact packing of few-layer nanosheets. The compact packing morphology caused by rolling and pressing processes forms sufficient pores for the penetration of electrolyte. For the preparation of asymmetric MoS_2||activated carbon supercapacitor, single-walled carbon nanotube (SWCNT) was used as the conducting agent to promote rapid ion transport, due to its high conductivity and stable nanochannel structure. 1T MoS_2 dispersion was first mixed and stirred with SWCNT dispersion with an active substance mass ratio of 8 : 2. Then the well-mixed dispersion was freeze-dried to obtain mixture powder. Through adding a small amount of water and PTFE (10% of the mixture powder mass), the MoS_2 electrode was prepared by rolling, freeze-drying and pressing the mixture powder into ~100 μm film with a high compaction density. To prepare the counter-electrode, YP-50 activated carbon, carbon black, carboxymethyl cellulose (CMC), and styrene-butadiene rubber (SBR) were mixed with a ratio of 85 : 9 : 2 : 4. The mixture was stirred in vacuum and evenly coated and pressed on a 22-μm-thick aluminum foil, then dried at 80 °C to obtain the counter electrode. The asymmetric supercapacitor was assembled by stacking and pressing 22-μm-thick aluminum foil (collectors), MoS_2 electrode (cathode), activated carbon electrode (anode), and glass fiber separator into a button supercapacitor cell. The mass loading of the cathode and anode are around 14.8 mg cm^{-2} and 10.2 mg cm^{-2}, respectively, which are adjusted based on the comprehensive matching of charge balance and electrode thickness.

Electrochemical measurements. Electrochemical measurements were carried out in a three-electrode configuration using an electrochemical workstation (PGSTAT302N, Metrohm Autolab B.V.). Ag/AgCl electrode and activated carbon were used as counter and reference electrodes, respectively. In order to make the comparison more convincing, we normalized the thickness and quality of the tested electrodes. During the three-electrode tests, CV (Cyclic Voltammetry) data were obtained at the voltage windows between -1 and 0.2 V vs. Ag/AgCl with the scan rates ranging from 5 to 1000 mV s^{-1}. For the asymmetric supercapacitor, the effective working voltage was chosen at 0 ~ 1.5 V with the scan rates of 1 ~ 100 mV s^{-1}.

The specific gravimetric capacitance (C_g, F g^{-1}) and the volumetric capacitance (C_v, F cm^{-3}) were calculated by the following formula, respectively:

$C_g = It / V$, (2)

$C_v = C_g \times \rho$, (3)

where I represents the mass normalized current (A g^{-1}), t is the discharge time (s) obtained in galvanostatic charge/discharge (GCD) measurements, V is the voltage window (V), and ρ is the density of tested electrode.

The energy and power densities of the supercapacitor were calculated by the following formula:

E (Wh g^{-1}) = $0.5 C_{cell} V_{cell}^2 / 3600$, (4)

E_v (Wh cm^{-3}) = $E \times \rho$, (5)

P (W g^{-1}) = $E \times 3600 / t_{cell}$, (6)

P_v (W cm^{-3}) = $P \times \rho$, (7)

where C_{cell} (F g^{-1}) is the total capacitance of asymmetric electrode cell, V_{cell} (V) is the effective working voltage of the discharging process, t_{cell} (s) is the discharging time, ρ (g cm^{-3}) is the normalized density of the two-electrode cell, E and P are specific energy and power density, respectively.

Declarations

Data availability. The data that support the findings of this study are available from the corresponding author upon request.

Acknowledgements

This work was supported by the National Natural Science Foundation of China (No. 51722604 and 51906211) and Royal Society Newton Advanced Fellowship (No. 52061130218). Z.B. acknowledges helpful discussion with Prof. Guang Feng (HUST).

Author contributions

Z.B., X.C. and H.Y. conceived the project. L.D., Z.H., J.Y. and K.C. discussed with Z.B., X.C. and H.Y. on the conceptualization of the work and experimental designs. Z.B., X.C. and H.Y. fabricated materials and performed experiments. Z.B., H.Y., X.G. and X.C. performed simulations and theoretical calculations. Z.B., X.C. and H.Y. analysed the data and interpreted the results. All the authors contributed to the writing of the manuscript.

Competing interests

The authors declare no competing interests.

Additional information

Supplementary information is available for this paper.

Correspondence and requests for materials should be addressed to Z.B.

Reprints and permission information is available at http://www.nature.com/reprints.

Publisher's note: Springer Nature remains neutral with regard to jurisdictional claims in published maps and institutional affiliations.

References

1. Pomerantseva, E., Bonaccorso, F., Feng, X., Cui, Y. & Gogotsi, Y. Energy storage: The future enabled by nanomaterials. *Science* **366**, eaan8285 (2019).
2. Choi, C. *et al.* Achieving high energy density and high power density with pseudocapacitive materials. *Nat. Rev. Mater.* **5**, 5–19 (2020).
3. Lethien, C., Le Bideau, J. & Brousse, T. Challenges and prospects of 3D micro-supercapacitors for powering the internet of things. *Energy Environ. Sci.* **12**, 96–115 (2019).
4. Sun, H. *et al.* Three-dimensional holey-graphene/niobia composite architectures for ultrahigh-rate energy storage. *Science* **356**, 599 (2017).
5. Gür, T. M. Review of electrical energy storage technologies, materials and systems: challenges and prospects for large-scale grid storage. *Energy Environ. Sci.* **11**, 2696–2767 (2018).
6. Kyerematen, N. A., Brousse, T. & Pech, D. Microsupercapacitors as miniaturized energy-storage components for on-chip electronics. *Nat. Nanotechnol.* **12**, 7–15 (2017).
7. Beidaghi, M. & Gogotsi, Y. Capacitive energy storage in micro-scale devices: recent advances in design and fabrication of micro-supercapacitors. *Energy Environ. Sci.* **7**, 867–884 (2014).
8. Kumar, K. S., Choudhary, N., Jung, Y. & Thomas, J. Recent Advances in Two-Dimensional Nanomaterials for Supercapacitor Electrode Applications. *ACS Energy Lett.* **3**, 482–495 (2018).
9. Anasori, B., Lukatskaya, M. R. & Gogotsi, Y. 2D metal carbides and nitrides (MXenes) for energy storage. *Nat. Rev. Mater.* **2**, 16098 (2017).
10. Feng, D. *et al.* Robust and conductive two-dimensional metal–organic frameworks with exceptionally high volumetric and areal capacitance. *Nat. Energy* **3**, 30–36 (2018).
11. Yu, D. *et al.* Scalable synthesis of hierarchically structured carbon nanotube–graphene fibres for capacitive energy storage. *Nat. Nanotechnol.* **9**, 555–562 (2014).
12. Lukatskaya, M. R. *et al.* Ultra-high-rate pseudocapacitive energy storage in two-dimensional transition metal carbides. *Nat. Energy* **2**, 6 (2017).
13. Fan, Z. *et al.* Modified MXene/Holey Graphene Films for Advanced Supercapacitor Electrodes with Superior Energy Storage. *Advanced Science* **5**, 1800750 (2018).

14. Acerce, M., Voiry, D. & Chhowalla, M. Metallic 1T phase MoS_2 nanosheets as supercapacitor electrode materials. *Nat. Nanotechnol.* **10**, 313–318 (2015).
15. Wang, Y., Yang, X., Pandolfo, A. G., Ding, J. & Li, D. High-Rate and High-Volumetric Capacitance of Compact Graphene–Polyaniline Hydrogel Electrodes. *Adv. Energy Mater.* **6**, 1600185 (2016).
16. Ghidiu, M., Lukatskaya, M. R., Zhao, M.-Q., Gogotsi, Y. & Barsoum, M. W. Conductive two-dimensional titanium carbide 'clay' with high volumetric capacitance. *Nature* **516**, 78–81 (2014).
17. Vijayakumar, M., Santhosh, R., Adduru, J., Rao, T. N. & Karthik, M. Activated carbon fibres as high performance supercapacitor electrodes with commercial level mass loading. *Carbon* **140**, 465–476 (2018).
18. Yang, X., Cheng, C., Wang, Y., Qiu, L. & Li, D. Liquid-Mediated Dense Integration of Graphene Materials for Compact Capacitive Energy Storage. *Science* **341**, 534–537 (2013).
19. Xu, Y. *et al.* Supercapacitors: A Metal-Free Supercapacitor Electrode Material with a Record High Volumetric Capacitance over 800 F cm^{-3}. *Adv. Mater.* **27**, 7898–7898 (2015).
20. Lin, T. *et al.* Nitrogen-doped mesoporous carbon of extraordinary capacitance for electrochemical energy storage. *Science* **350**, 1508–1513 (2015).
21. Choi, W. *et al.* Recent development of two-dimensional transition metal dichalcogenides and their applications. *Mater. Today* **20**, 116–130 (2017).
22. Zhang, G., Liu, H., Qu, J. & Li, J. Two-dimensional layered MoS2: rational design, properties and electrochemical applications. *Energy Environ. Sci.* **9**, 1190–1209 (2016).
23. Jiao, Y. C. *et al.* Metallic MoS_2 for High Performance Energy Storage and Energy Conversion. *Small* **14**, 1800640 (2018).
24. Kappera, R. *et al.* Phase-engineered low-resistance contacts for ultrathin MoS_2 transistors. *Nat. Mater.* **13**, 1128–1134 (2014).
25. Py, M. A. & Haering, R. R. Structural destabilization induced by lithium intercalation in MoS_2 and related compounds. *Can. J. Phys.* **61**, 76–84 (1983).
26. Acerce, M., Akdogan, E. K. & Chhowalla, M. Metallic molybdenum disulfide nanosheet-based electrochemical actuators. *Nature* **549**, 370–373 (2017).
27. Eda, G. *et al.* Photoluminescence from Chemically Exfoliated MoS2. *Nano Lett.* **11**, 5111–5116 (2011).
28. Sarkar, D. *et al.* Expanding Interlayer Spacing in MoS_2 for Realizing an Advanced Supercapacitor. *ACS Energy Lett.* **4**, 1602–1609 (2019).
29. Zhou, J. *et al.* 1T-MoS_2 nanosheets confined among TiO_2 nanotube arrays for high performance supercapacitor. *Chem. Eng. J.* **366**, 163–171 (2019).
30. Liu, Q. *et al.* Gram-Scale Aqueous Synthesis of Stable Few-Layered 1T-MoS_2: Applications for Visible-Light-Driven Photocatalytic Hydrogen Evolution. *Small* **11**, 5556–5564 (2015).

31. Voiry, D., Mohite, A. & Chhowalla, M. Phase engineering of transition metal dichalcogenides. *Chem. Soc. Rev.* **44**, 2702–2712 (2015).
32. Shi, S. L., Sun, Z. X. & Hu, Y. H. Synthesis, stabilization and applications of 2-dimensional 1T metallic MoS_2. *J. Mater. Chem. A* **6**, 23932–23977 (2018).
33. Yu, Y. F. *et al.* High phase-purity 1T'-MoS_2- and 1T'-$MoSe_2$- layered crystals. *Nat. Chem.* **10**, 638–643 (2018).
34. Liu, L. N. *et al.* Phase-selective synthesis of 1T ' MoS_2 monolayers and heterophase bilayers. *Nat. Mater.* **17**, 1108–1114 (2018).
35. Chen, X. Y. *et al.* High Phase-Purity 1T-MoS2 Ultrathin Nanosheets by a Spatially Confined Template. *Angew. Chem.-Int. Edit.* **58**, 17621–17624 (2019).
36. Perdew, J. P. *et al.* Atoms, molecules, solids, and surfaces: Applications of the generalized gradient approximation for exchange and correlation. *Physical Review B* **46**, 6671–6687 (1992).
37. Perdew, J. P., Burke, K. & Ernzerhof, M. Generalized gradient approximation made simple. *Phys Rev Lett* **77**, 3865–3868 (1996).
38. Kan, M. *et al.* Structures and Phase Transition of a MoS2 Monolayer. *J. Phys. Chem. C* **118**, 1515–1522 (2014).
39. Chen, Y. *et al.* Phase engineering of nanomaterials. *Nature Reviews Chemistry* (2020).
40. Kong, J. *et al.* High-Mass-Loading Porous $Ti_3C_2T_x$ Films for Ultrahigh-Rate Pseudocapacitors. *ACS Energy Lett.* **5**, 2266–2274 (2020).
41. Pech, D. *et al.* Ultrahigh-power micrometre-sized supercapacitors based on onion-like carbon. *Nat. Nanotechnol.* **5**, 651–654 (2010).
42. El-Kady, M. F. & Kaner, R. B. Scalable fabrication of high-power graphene micro-supercapacitors for flexible and on-chip energy storage. *Nat. Commun.* **4**, 1475 (2013).
43. Zhong, J. *et al.* Efficient and scalable synthesis of highly aligned and compact two-dimensional nanosheet films with record performances. *Nat. Commun.* **9**, 3484 (2018).
44. Lukatskaya, M. R. *et al.* Cation Intercalation and High Volumetric Capacitance of Two-Dimensional Titanium Carbide. *Science* **341**, 1502–1505 (2013).
45. Liu, M., Niu, J., Zhang, Z., Dou, M. & Wang, F. Potassium compound-assistant synthesis of multi-heteroatom doped ultrathin porous carbon nanosheets for high performance supercapacitors. *Nano Energy* **51**, 366–372 (2018).
46. Li, H. *et al.* Flexible All-Solid-State Supercapacitors with High Volumetric Capacitances Boosted by Solution Processable MXene and Electrochemically Exfoliated Graphene. *Adv. Energy Mater.* **7**, 1601847 (2017).
47. Wu, Z. S., Parvez, K., Feng, X. & Müllen, K. Graphene-based in-plane micro-supercapacitors with high power and energy densities. *Nat. Commun.* **4**, 2487 (2013).
48. Kresse, G. & Furthmuller, J. Efficient iterative schemes for ab initio total-energy calculations using a plane-wave basis set. *Phys Rev B* **54**, 11169–11186 (1996).

49. Kresse, G. & Furthmuller, J. Efficiency of ab-initio total energy calculations for metals and semiconductors using a plane-wave basis set. *Comp Mater Sci* **6**, 15–50 (1996).

Figures

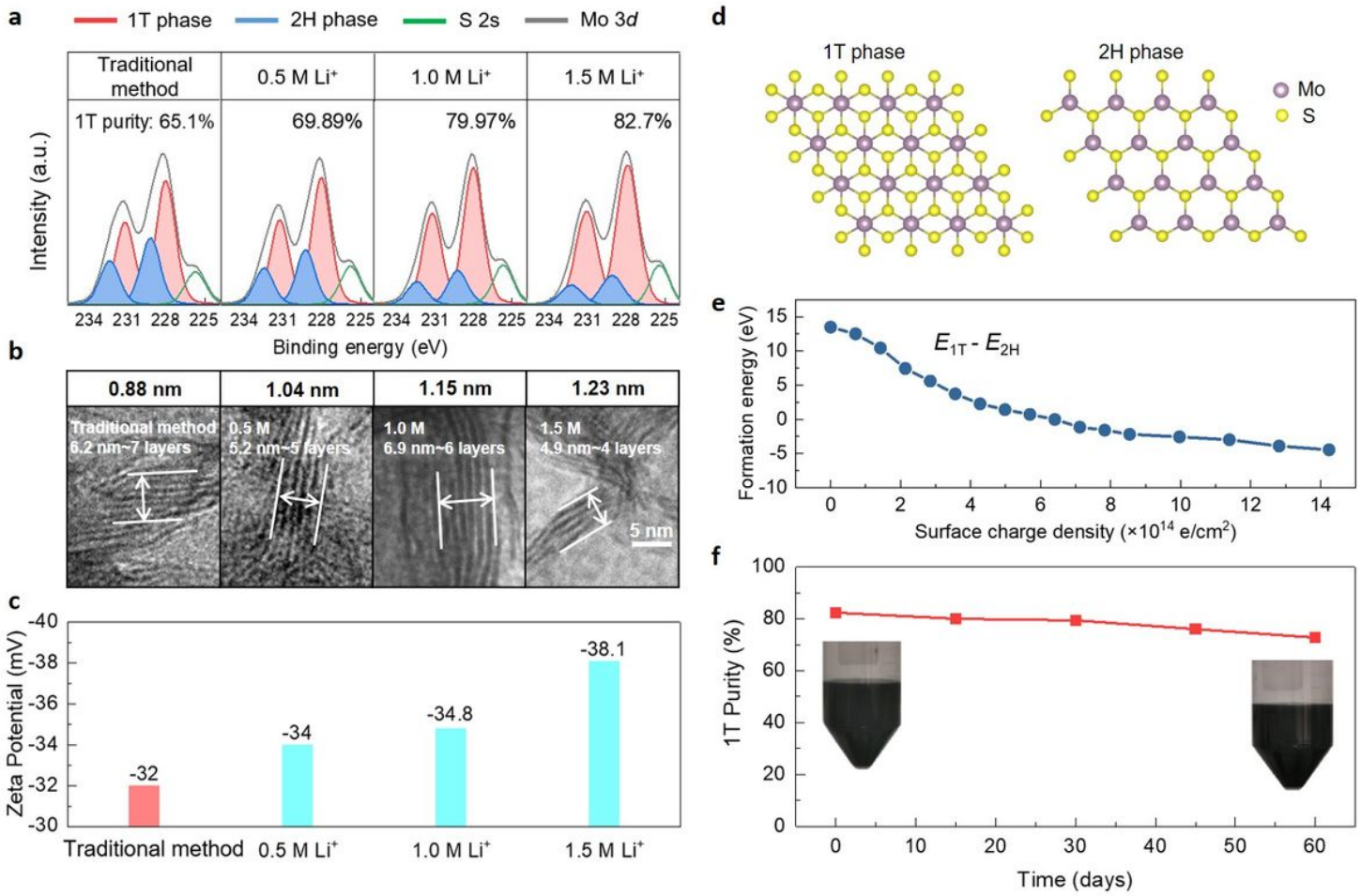

Figure 2

Schematic of characterization and theoretical calculations of Li+-intercalated 1T MoS2. a,b, XPS spectrums (a) of Mo 3d and zeta potentials (b) of 1T MoS2 nanosheets (black) by traditional hydrothermal method and our strategy with different Li+ concentrations. Contributions of 1T and 2H phase components are indicated by red and blue regions, respectively. d, Geometric structures of 1T and 2H phase MoS2 in the DFT calculation. e, The DFT-calculated formation-energy difference between 1T and 2H phase MoS2 with the increase of negative charges. f, 1T purity attenuation of Li+-intercalated MoS2 dispersion. Inset shows that the dispersion remains stable without the obvious precipitation within 60 days.

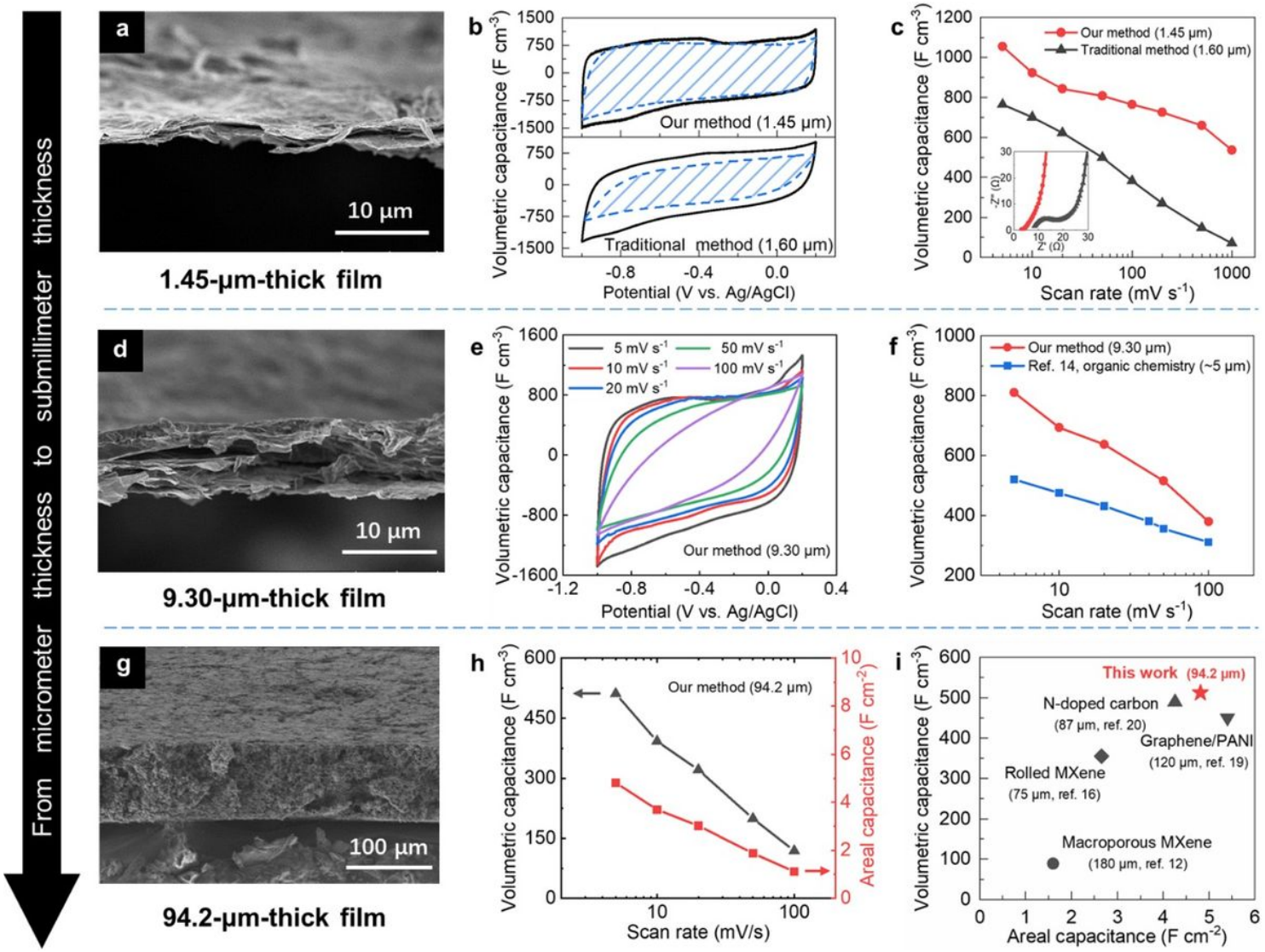

Figure 3

Electrochemical performance of Li+-intercalated MoS2 films from micrometer thickness to submillimeter thickness. a, A cross-sectional SEM image of the 1.45-μm-thick MoS2 film. b,c, Segregation of surface capacitive and diffusion-limited contributions for the CV at 20 mV s-1 (b) and rate capabilities (c) of MoS2 films prepared by traditional hydrothermal method and our strategy. d,e, A cross-sectional SEM image (d) and CV curves at scan rates from 5 to 100 mV s-1 (e) of the 9.30-μm-thick MoS2 film. f, A comparison of rate capability between MoS2 films by traditional hydrothermal method and our strategy. g,h, A cross-sectional SEM image (g) and the rate capability of the volumetric and areal capacitances (h) for the 94.2-μm-thick MoS2 film. i, Comparison of the volumetric and areal capacitance of the 94.2-μm-thick MoS2 film (red mark) with the performance of other nanomaterial electrodes with similar thickness.

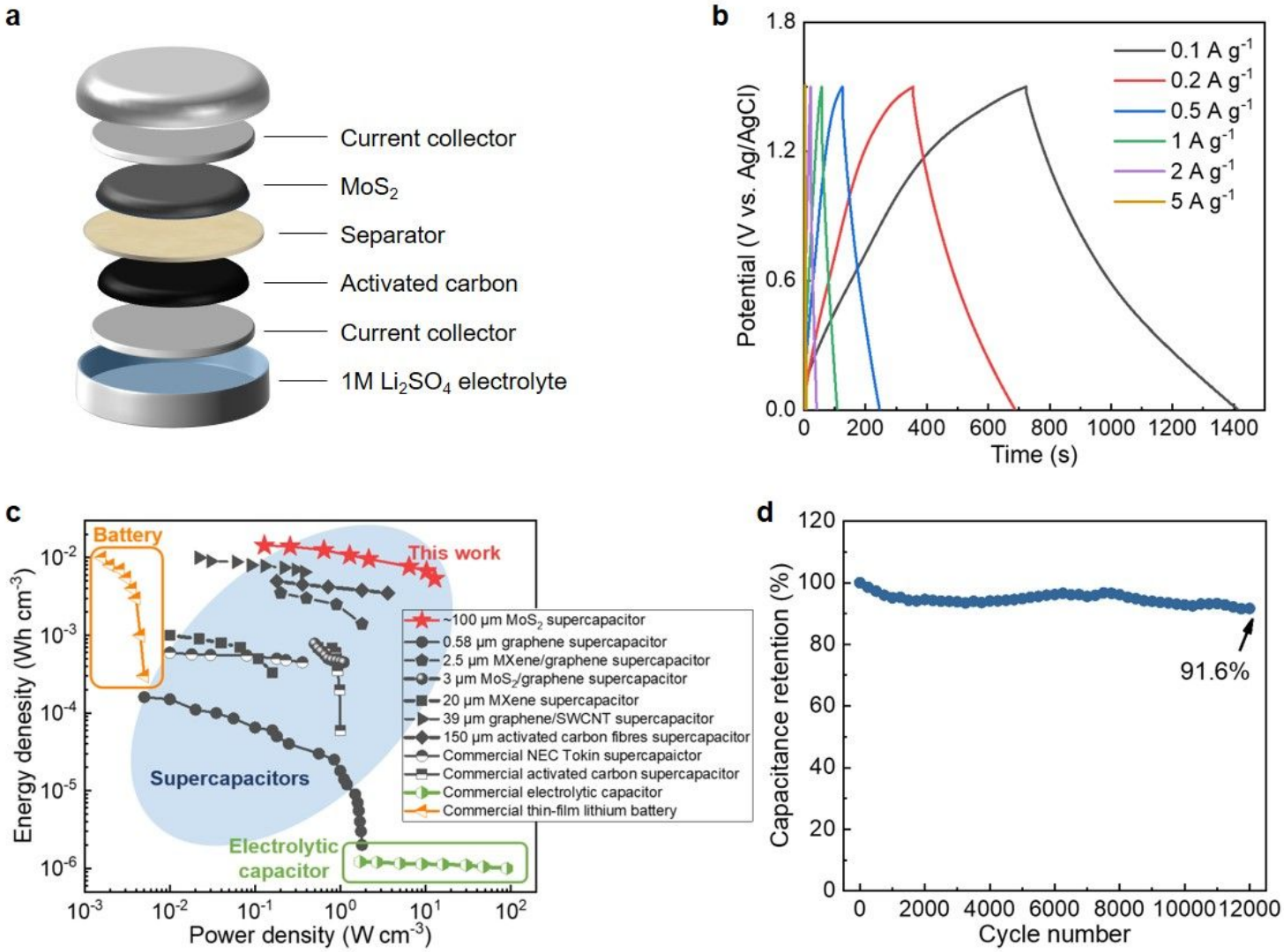

Figure 4

Asymmetric MoS2||activated carbon supercapacitor with high energy and power densities. a,b, Schematic (a) and GCD curves (b) of the asymmetric MoS2||activated carbon supercapacitor. c, Ragone plot of the volumetric power and energy densities of our device in comparison with commercial devices and previous studies. d, Cycling stability test of the asymmetric MoS2||activated carbon supercapacitor.

Supplementary Files

This is a list of supplementary files associated with this preprint. Click to download.

- SupplementaryInformation.docx